Enhancement of Surfactants in Nanoparticles Produced by an Electrospray Aerosol Generator

Amanda C. MacMillan,[1] John B. Morrison,[1] Christopher W. Harmon,[1,2] and Sergey A. Nizkorodov[1]

[1]*Department of Chemistry, University of California, Irvine, California, USA*
[2]*Department of Chemistry, Humboldt State University, Arcata, California, USA*

Electrospray aerosol generators (EAGs) disperse conducting solutions into air, promptly neutralize the particles to remove the excess charge, and evaporate the residual solvent with a dry air flow. For solutions containing multiple solutes, the particles may become enhanced in the more surface-active solutes. The extent of the enhancement was estimated for nanoparticles electrosprayed from a solution containing NaCl and surfactant sodium dodecyl sulfate (SDS) mixed in a 9:1 weight ratio. A tandem particle mobility analyzer was used to quantify the hygroscopic growth factor (*GF*). The relative fractions of NaCl and SDS in the particles were estimated from the measured *GFs* assuming that NaCl and SDS take up water independently of each other. The nanoparticles were considerably enhanced in SDS relative to the starting solution, with the NaCl:SDS weight ratio increasing with the distance from the EAG electrified capillary tip to the neutralizer, and reaching ∼1:1 at the longest distances probed. The enhancement in SDS likely occurred during particle fission events as particles traveled from the capillary to the neutralizer. This study has practical ramifications for aerosol nanotechnology and aerosol-assisted drug delivery, which rely on EAG as an instrument of choice for nanoparticle generation.

[Supplementary materials are available for this article. Please go to the publisher's online edition of *Aerosol Science and Technology* to view the free supplementary files.]

1. INTRODUCTION

Electrospray is a process of creating small highly charged droplets by dispersing a conducting solution through an electrified capillary. In electrospray ionization (ESI), the conditions are optimized for mass spectrometric analysis so that the droplets

disintegrate down to individual ions through a series of droplet fission and solvent/ion evaporation steps (Kebarle and Peschke 2000; Kebarle and Verkerk 2010). An electrospray aerosol generator (EAG) employs a somewhat different set of conditions to produce particles in the nanometer to micron size range (Rulison and Flagan 1994; Tang and Gomez 1994; Chen et al. 1995; Modesto-Lopez et al. 2011). Generally, this is achieved by keeping the solution concentrations several orders of magnitude higher than in ESI (mM vs. μM) and removing the excess charge from the particles immediately after the electrospray process.

Under appropriately chosen conditions, such as capillary flow and applied potential, electrospray operates in a cone-jet mode (Jaworek and Sobczyk 2008), in which the liquid exiting the capillary forms a sharp conical tip, known as the Taylor cone. As first described by Taylor (1964), charged primary droplets containing both the solutes and solvent break off from the Taylor cone and travel toward the nearest grounded surface. It is believed that solvent evaporation causes shrinkage of these primary droplets, which leads to asymmetric fission events at the Rayleigh space-charge limit and result in a release of several *progeny* droplets (Kebarle and Peschke 2000). The progeny droplets carry only a fraction of the primary particle mass and remove a substantial fraction of its charge. These processes take place on a millisecond time scale, and by the time the droplets reach the grounded surface several evaporation/fission cycles may have already occurred (Figure 1). In EAG applications, droplet fission is typically suppressed by injecting the droplets directly into a weak plasma (Lu and Koropchak 2004), which facilitates the flow of the excess charge between the droplets and the surrounding metal surfaces.

As the progeny droplets break off from the apex of a distorted primary droplet they may become enriched with the more surface-active solute. It is well known that ESI sources preferentially generate ions corresponding to molecules with high surface activities due to the interplay between surface charge and surface tension (Cech and Enke 2001). An enhancement in the surface-active species in nanoparticles generated by EAG has also been noted in previous work (Tang and Smith 2001;
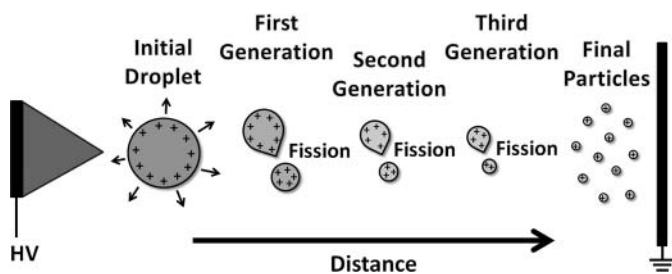
FIG. 1.   Cartoon of the fission process droplets undergo as they break off from the Taylor cone and travel (left to right) toward the neutralizer.

Alshawa et al. 2009; Harmon et al. 2010). Several experimental parameters are expected to affect the enhancement, including the capillary voltage, capillary (i.e., liquid) flow rate, drying air flow rate, and the distance (l_s) of the electrospray capillary tip to the neutralizing surface. To the best of our knowledge, the effect of these parameters on the enhancement of surface-active species in nanoparticles has not been systematically investigated. One relevant study was conducted by Schmidt et al. (2003), who examined the effect of liquid flow rates on the ESI mass spectra of solutions containing solutes with significant differences in surface activities. They observed a strong suppression of the signal intensity of hydrophilic solutes with decreasing flow rate. They attributed this effect to smaller initial droplet sizes obtained at reduced flows resulting in a greater chance that surface-active solutes would remain in progeny droplets during fission events. Another relevant study by Benkestock et al. (2004) investigated the effect of changing various electrospray parameters, including l_s, on the concentration of noncovalently bound complexes between proteins and small organic ligands. They found that the protein-ligand complex to free protein ratio increased with l_s when a hydrophilic ligand was used, whereas the opposite trend was observed using hydrophobic ligands. They attributed this effect to preferential sampling of ions from the bulk of the primary droplet through formation of late-generation residue droplets at large values of l_s.

The goal of this work is to investigate the effect of l_s on the enhancement of surface-active species in nanoparticles produced by an EAG. We rely on tandem hygroscopic growth factor (GF) measurements (Rader and McMurry 1986) of EAG-generated nanoparticles as an indirect way to probe their chemical composition. The particles contain an ionic surfactant, sodium dodecyl sulfate (SDS), with small hygroscopic GF values and a hygroscopic salt, NaCl, with large GF values. When exposed to a well-defined relative humidity (RH), the particles grow in size due to uptake of water by NaCl. The particles' GF is measured experimentally as the ratio of the mobility-equivalent diameter of the wet particles, $d_{m,\text{wet}}(RH)$, to the mobility-equivalent diameter of the dry particles, $d_{m,\text{dry}}$:

$$GF(RH) = \frac{d_{m,\text{wet}}(RH)}{d_{m,\text{dry}}}   [1]$$

Assuming that NaCl and SDS take up water independently in proportion to their corresponding volume fractions, the amount of SDS in the particles at any RH can be estimated from the GF and assumed particle morphology. We will show that increasing the distance between the capillary tip and the neutralizer increases the relative amount of SDS in the nanoparticles. These results are consistent with the hypothesis that progeny droplets, formed from the fission events of primary droplets, are enriched with the surface-active species present.

2.   EXPERIMENTAL

Nanoparticles were generated using a custom-built EAG described in detail elsewhere (Alshawa et al. 2009; Harmon et al. 2010). The electrosprayed SDS/NaCl solution was prepared using NaCl (Sigma-Aldrich, 99.999%) and SDS (Fluka, ≥99.0%) dissolved in HPLC grade water (OmniSolv, <8 $\mu\Omega$ cm), with a small volume (<5%) of methanol (Sigma-Aldrich, HPLC grade) to stabilize the electrospray cone. The solute consisted of 10.7 wt% SDS and 89.3 wt% NaCl (solute molar fractions of 0.0237 and 0.976, respectively). The combined SDS + NaCl weight concentration in the solution was 2.1 g L^{-1}, resulting in solution concentrations of SDS and NaCl of 0.78 and 32 mM, respectively. The electrosprayed solution of pure NaCl was prepared by dilution of NaCl in HPLC grade water and a small volume (<5%) of methanol. The SDS and NaCl are both soluble in water and have solubility values of 150 and 359 g L^{-1}, respectively. The SDS is capable of forming micelles; however, its critical micelle concentration is 8.2 mM at 298 K. Therefore, no micelles are expected in the initial solution used in the experiments.

Using a syringe pump, solutions were pushed through a capillary tube (360 μm outer diameter [o.d.], 100 μm inner diameter [i.d.]) at a rate of ∼80 μL h^{-1} at 295 K. The capillary was housed in a 5 cm^3 chamber, with transparent windows to allow for viewing the electrospray (Figure 2a). A positive potential (∼4 kV) was applied to the capillary to produce a stable cone-jet. The spray was carried by a ∼1 SLM (standard liter per minute) flow of dry air toward the entrance of an electrically-grounded neutralizer (^{85}Kr, 10 mCi, TSI Model 3077A, 6.4 mm o.d., 4.8 mm i.d.). The distance from the capillary tip to the entrance of the neutralizer (l_s) was varied from 4 to 10 mm in approximately 0.3 mm increments with a linear translation stage. After exiting the neutralizer, the number concentrations of polydisperse nanoparticles were typically in excess of 10^5 particles cm^{-3}.

Nanoparticles were size selected and their GFs were measured using a hygroscopicity tandem differential mobility analysis (HTDMA) method described elsewhere (Alshawa et al. 2009; Harmon et al. 2010). The initial dry mobility-equivalent diameter was selected using the first differential mobility analyzer (DMA1, TSI Model 3085) operated under dry conditions (RH <1%). A fixed DC voltage was applied to DMA1 in order to select a narrow distribution of mobility-equivalent diameter ($d_{m,\text{dry}}$) = 14.5 (±0.1) nm (with a geometric standard deviation
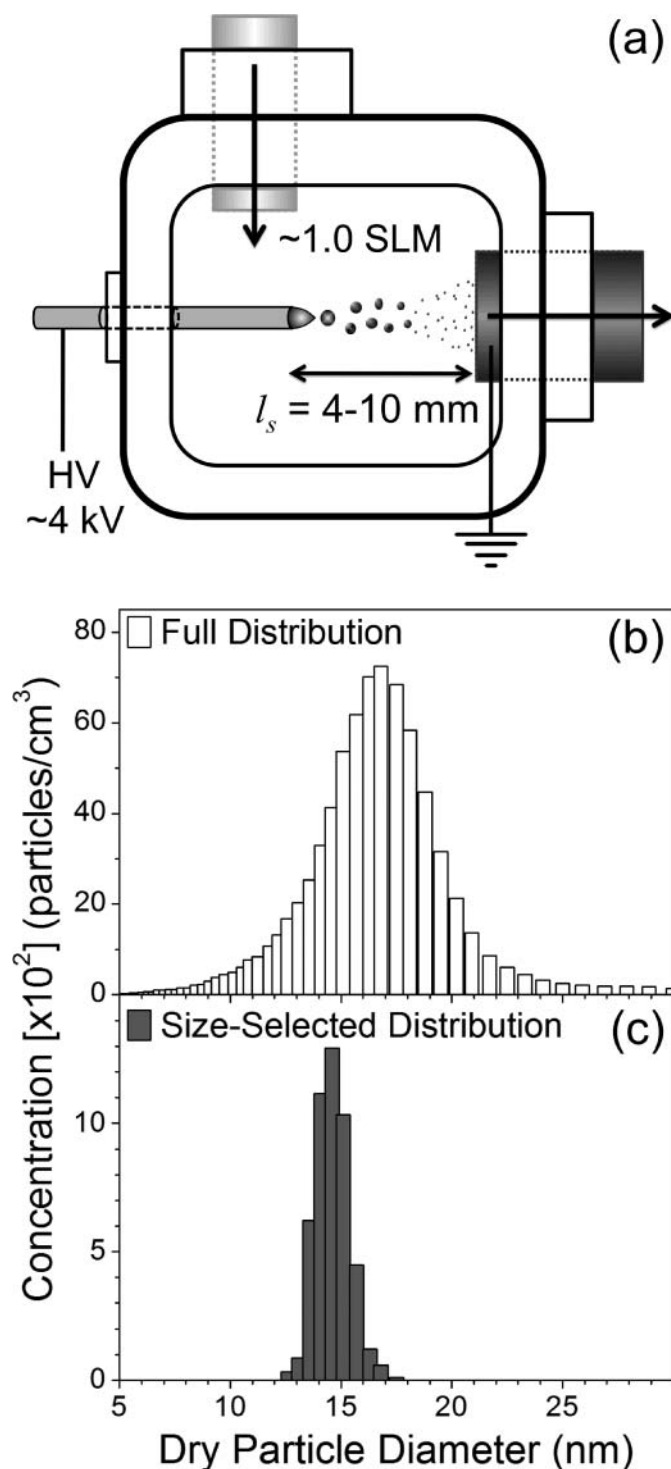
FIG. 2. (a) Schematic diagram of the electrospray housing chamber. An SDS/NaCl solution is pushed through a capillary and electrosprayed. Droplets are carried toward the neutralizer opening (dark grey cylinder on right) with a flow of dry air. The double-sided arrow indicates the capillary tip to neutralizer distance (l_s), which is varied in the experiments. (b) Full particle mobility-equivalent size distribution of the SDS/NaCl particles measured by the first DMA and (c) after size-selection for 14.5 nm SDS/NaCl particles using the second DMA.

of ∼1.06). This particular size was chosen because it was near the peak of the full size distribution for the particles generated by the EAG, thus maximizing the particle count. The selected particles were then passed through a humidifier (90% RH) and entered the second DMA (DMA2, TSI Model 3085) for sizing. The sheath flow of DMA2 was also humidified to 90% RH. Following the particle mobility-equivalent diameter measurements with DMA2, the particles were detected with an ultrafine condensation particle counter (TSI Model 3025A).

DMA2 was operated in a scanning mobility particle sizer (SMPS) mode, wherein the voltage applied to the central rod was scanned using the electrostatic classifier (TSI Model 3080) controlled by TSI Aerosol Instrument Manager software (version 9.0). We should note that the assumptions made by the data inversion algorithms used by the SMPS software may lead to inaccurate results for sizing particles in HTDMA experiments. As discussed by Rader and McMurry (1986), in cases where the particle number concentration changes significantly over the size range transmitted by the fixed-voltage DMA1, the peak in the particles' size distribution measured by the DMA2 will be shifted from the actual average size of the particles. A proper way to correct for these effects is to use a data inversion algorithm designed specifically for HTDMA (Rader and McMurry 1986), such as TDMAFIT (Stolzenburg and McMurry 1988). However, one can also minimize these effects by size-selecting particles with DMA1 close to the peak of the initial size distribution produced by the EAG. In the experiments described in this work, we adopted the latter approach. While the absolute *GF* values may be slightly off, the change in *GF* measured in this way should be reasonably accurate.

3. RESULTS AND DISCUSSION

A typical size distribution of the SDS/NaCl particles exiting the neutralizer is shown in Figure 2b. The distribution is plotted as a function of the average mobility-equivalent diameter that penetrates through the DMA2 based on the voltage applied to its central rod. The mean mobility-equivalent diameter for the full particle distribution (∼16 nm) is close to the particle diameter of 24 nm predicted from the EAG scaling laws by Chen et al. (1995). The mean diameter did not change significantly as the capillary-neutralizer distance l_s was varied. The corresponding distribution for the pure NaCl particles (not shown) was similar. We have not verified whether the particles have achieved the equilibrium Boltzmann charge distribution after the neutralizer, but the monomodal shape of the distribution suggests that all particles passing through DMA1 are singly-charged, an important prerequisite for the HTDMA measurements. If multiply-charged particles were present, a multimodal size distribution would have been observed (Modesto-Lopez et al. 2011).

In conventional EAG sources, neutralization was accomplished with [210]Po neutralizers (Chen et al. 1995; Scalf et al. 1999). This work suggests that [85]Kr neutralizers are also suitable for EAG sources (in fact, we found no significant differences

in measured size distributions when the [85]Kr neutralizer was replaced with a [210]Po neutralizer). Figure 2c shows an example of a size distribution for the dry SDS/NaCl particles that were size-selected by DMA1 and measured by DMA2. The size distribution corresponding to the size-selected and humidified particles was similar but shifted toward higher mobility diameter by a factor of *GF*.

Harmon et al. (2010) investigated the hygroscopic growth for nanoparticles of pure NaCl, pure SDS, and variable SDS/NaCl content over the RH range of 1–95%. The *GF* values of the particles with variable SDS/NaCl content measured in that study implied that the relative fractions of SDS in the nanoparticles were significantly higher than the corresponding SDS fractions in the initial solution. In order to provide a more definite proof of the SDS enhancement, we performed experiments in which the RH and solution composition were fixed and only l_s was varied. To simplify the quantitative analysis of the measured *GF* values, the RH was also fixed at 90%, which is above the deliquescence RH of NaCl. At this RH value, all NaCl in the particles should be fully deliquesced.

The change in *GF* as a function of capillary distance is shown in Figure 3a. As expected, the *GF* of the pure NaCl particles remains unchanged as l_s increases. As noted in the experimental section, the absolute value of the *GF*s may be slightly off because the initial particles' size distribution generated by the EAG is comparable in width to the transfer function of the DMA (Rader and McMurry 1986). Nevertheless, the measured value is in qualitative agreement with previous *GF* measurements for NaCl nanoparticles by other research groups (Hameri et al. 2001; Biskos et al. 2006a,b). For example, the theoretical *GF* = 1.87 for pure NaCl at 90% RH, calculated using "Model 4" from Biskos et al. (2006b), is in good agreement with the experimental results.

Calculating the theoretical *GF* for the SDS/NaCl particles at 90% RH is a challenge because of the uncertainty regarding the exact amount of SDS in the final particles. However, it can be estimated using the experimental *GF* values and the Zdanovskii−Stokes−Robinson (ZSR) model (Stokes and Robinson 1966; Svenningsson et al. 2006; Varutbangkul et al. 2006). The ZSR model assumes that the overall growth of a mixed SDS/NaCl particle is entirely due to independent water uptake by the different particle components. As pure SDS does not measurably grow at the RH values probed in this work (Harmon et al. 2010), we can write the following simplified ZSR equation:

$$GF^3 = \varepsilon_{\mathrm{SDS}} GF_{\mathrm{SDS}}^3 + \varepsilon_{\mathrm{NaCl}} GF_{\mathrm{NaCl}}^3 \approx 1 + \varepsilon_{\mathrm{NaCl}} \left(GF_{\mathrm{NaCl}}^3 - 1 \right) \quad [2]$$

Here, GF_{SDS} and GF_{NaCl} are the *GF* values for the particles made of pure SDS and NaCl, respectively, and $\varepsilon_{\mathrm{SDS}}$ and $\varepsilon_{\mathrm{NaCl}}$ are the volume fractions of SDS and NaCl in the mixed particle. The *GF* = 1.80 value for the SDS/NaCl mixture predicted from Equation (2) is much larger than the experimentally ob-
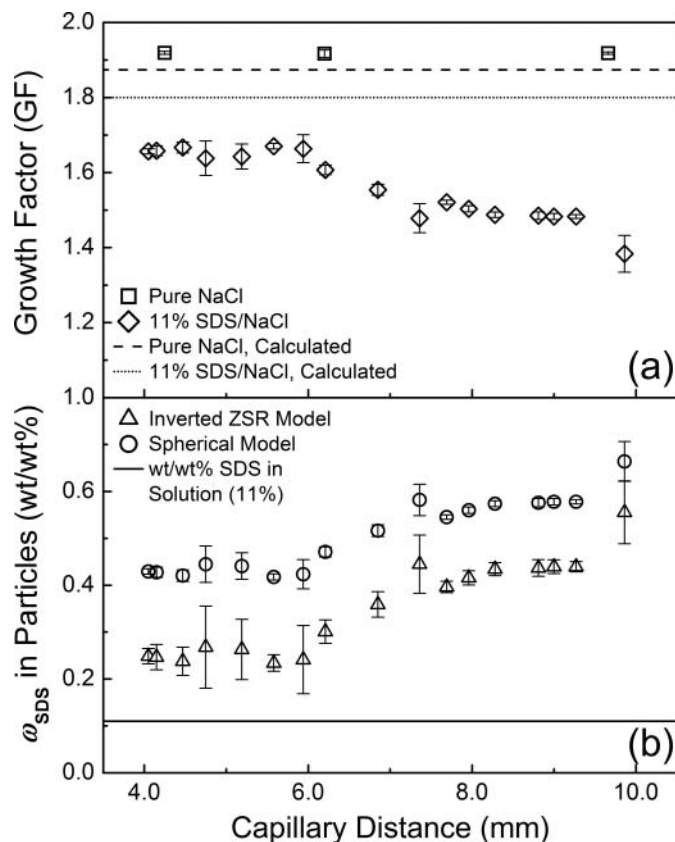

FIG. 3. (a) Measured *GFs* of SDS/NaCl particles and pure NaCl particles at 90% RH as a function of the capillary distance. As the capillary distance increases, *GFs* of SDS/NaCl particles decrease, whereas the *GF* of pure NaCl remains unchanged. The dashed line represents the *GF* = 1.87 calculated for pure NaCl using "Model 4" from Biskos et al. (2006b). The dotted line represents the *GF* = 1.80 expected for the SDS/NaCl particles from ZSR model, Equation (2), assuming that particles have the same SDS/NaCl proportion as the electrosprayed solution. (b) Weight fraction of SDS (ω_{SDS}) in the nanoparticles calculated from the measured *GF* values using the inverted ZSR model, Equation (4), and the Spherical Model described in the SI. The straight line represents the ω_{SDS} in the initial solute (0.11). The relative amount of SDS in the particle is approximately enhanced by a factor of 4–6.

served values shown in Figure 3a implying that the particles are depleted in NaCl or, equivalently, enhanced in SDS.

Furthermore, in contrast to the *GF* of the pure NaCl particles, the *GF* values of the SDS/NaCl particles reproducibly decrease as l_s increases, despite the fact that particles of the same mobility are selected by DMA1 *prior to* the humidification. As pure SDS nanoparticles exhibit almost no hygroscopic growth at this RH (Harmon et al. 2010), all of the particle growth in the mixed case must be due to equilibrium water uptake of the NaCl component. To explain the observations, we have to assume that particles formed at larger l_s must have larger weight fractions of SDS (ω_{SDS}), defined as $\omega_{\mathrm{SDS}} = m_{\mathrm{SDS}}/(m_{\mathrm{NaCl}} + m_{\mathrm{SDS}})$, where m_{SDS} and m_{NaCl} are the masses of SDS and NaCl in the particles, respectively. These larger values of ω_{SDS} at larger l_s agree with the expected mechanism of particle formation for EAGs

(Figure 1). The goal of the following discussion is to estimate ω_{SDS} from the measured *GF* data, and compare it with the solution's initial ω_{SDS} of 0.11 (corresponding to the initial dry mole fraction of 0.024 for SDS).

A direct measurement of the amounts of SDS and NaCl in the nanoparticles is difficult due to the miniscule amount of particulate material produced by EAGs. Under the optimal conditions, our EAG produces about 10^5 particles cm^{-3} in a 1 SLM flow or about 100 ng of 20 nm particles per hour of operation. Our previous attempts to quantify the Cl to S ratio in these particles using X-ray photoelectron spectroscopy did not succeed (Harmon et al. 2010). However, the relative amounts of SDS and NaCl can be obtained indirectly from the ZSR model, Equation (2). The measured *GFs* at every capillary distance (Figure 3a) can be converted into the volume fractions of NaCl through an inversion of Equation (2):

$$\varepsilon_{NaCl} \approx \frac{GF^3 - 1}{GF_{NaCl}^3 - 1} \qquad [3]$$

Then, these can be converted into the corresponding weight fractions of NaCl (ω_{NaCl}),

$$\omega_{NaCl} \approx \frac{\varepsilon_{NaCl} \cdot \rho_{NaCl}}{\rho_{SDS} + \varepsilon_{NaCl} \cdot (\rho_{NaCl} - \rho_{SDS})} \qquad [4]$$

using the bulk densities of $\rho_{NaCl} = 2163$ kg m^{-3} and $\rho_{SDS} = 1010$ kg m^{-3}. We note that using this particular density for SDS is a simplification in view of the large number of its possible solid phases (Sperline 1997). The estimated values of $\omega_{SDS} = 1 - \omega_{NaCl}$ are shown in Figure 3b as a function of l_s. They are significantly larger than the initial ω_{SDS} of 0.11 in the electrosprayed solution, and increase with l_s.

The above estimation is rather crude as it does not take into account the difference in the shapes of the dry NaCl and SDS/NaCl particles and neglects the Kelvin effect. Furthermore, deviations from the ZSR model may occur when the interactions between different phases within the particle are significant. The ZSR model was found to perform poorly in the case of submicron SDS/NaCl particles interacting with water vapor below the deliquescence transition, in part due to the complicated shapes of the mixed particles (Zelenyuk et al. 2007). A more accurate (although still approximate) estimation of ω_{SDS} can be done as described in the Supplementary Information (SI). The values of ω_{SDS} calculated with the formulas in the SI are also shown in Figure 3b.

As shown in Figure 3b, the values of ω_{SDS} approximated from the ZSR model and from the more refined model described in the SI suggest a significant enhancement of SDS in the final nanoparticles. The ratio of the weight concentrations of SDS and NaCl in the initial solution is about 1:9 (the corresponding molar ratio is about 1:40). The same proportion of SDS and NaCl in the particles would correspond to a ω_{SDS} of 0.11, a value indicated in Figure 3b by a thick horizontal line. While

approximate, the calculations suggest that the actual ω_{SDS} values might range from ~0.4 at the smallest l_s (4 mm) to ~0.6 at the largest l_s (10 mm). As discussed in more detail below, this behavior is consistent with the model in which particle fission events produce progeny droplets enriched with surface-active species. The effect on the particle composition is quite dramatic. At the largest values of the distance between the EAG capillary and the neutralizer (10 mm), the estimated SDS:NaCl weight ratio in the particles exceeds 1:1 (molar ratio 1:5), which is very different from the initial solution.

We also conducted experiments in which the capillary to neutralizer distance was fixed but the initial dry mobility-equivalent diameter of the particles was varied. Figure 4a shows the measured *GF* values at 90% RH and Figure 4b shows the corresponding ω_{SDS} values plotted as a function of the initial dry particle mobility-equivalent diameter. We find that smaller particles tend to contain more SDS, although the particles' size dependence is not very pronounced for the probed initial mobility sizes of 11–17 nm.
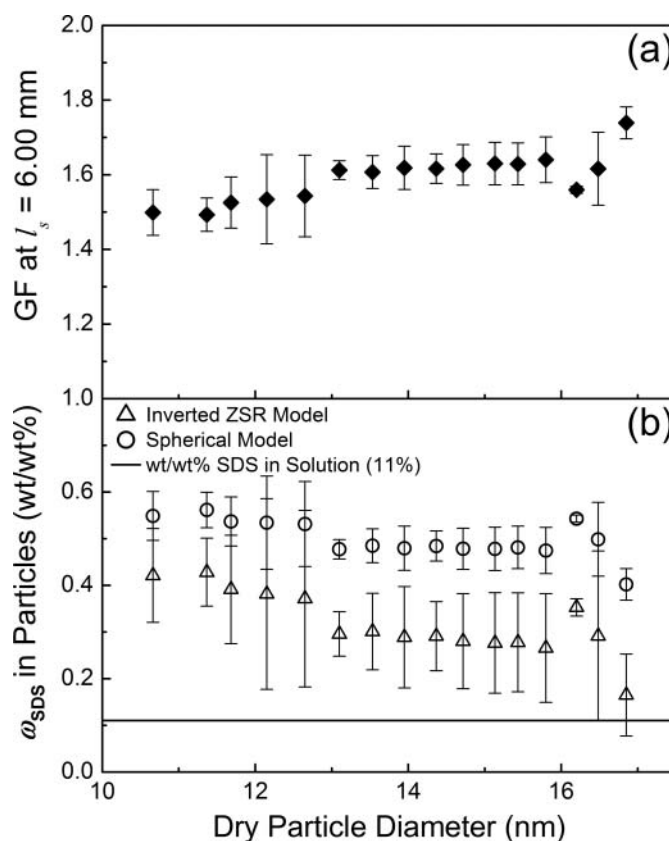

FIG. 4. (a) Measured *GFs* of SDS/NaCl particles at a fixed capillary distance (6.00 mm) for various initial dry particle mobility-equivalent diameters (nm) at 90% RH. (b) Calculated weight fraction of SDS (ω_{SDS}) in the nanoparticles using the inverted ZSR model, Equation (4), and the Spherical model described in the SI. The straight line represents the ω_{SDS} in the initial solute (0.11). As the initial particle diameter increases, measured *GF* increases and the ω_{SDS} in the particle decreases.

These observations can be rationalized with a simple conceptual model. With the initial solution composition used in this study, the primary droplets formed by the electrospray should have enough surface area to accommodate *all* of the SDS molecules on the surface (all droplets below about 30 μm in size will be under-saturated with respect to the full surface coverage of 4×10^{-10} mol cm^{-2} measured by Iyota and Krastev [2009]). If we assume that all of the SDS and NaCl reside on the droplet surface and interior, respectively, and that the SDS surface distribution can instantaneously adjust during droplet distortions, we can expect significant SDS enhancement during an asymmetric droplet fission. For example, if we start with a 1 μm primary droplet with $\omega_{SDS} = 0.11$, and let the primary droplet undergo an asymmetric fission into a 0.1 μm progeny droplet, the new ω_{SDS} in the progeny droplet has the potential to increase by a factor of five. Comparison with the data shown in Figures 3b and 4b suggest the observed SDS enhancement can result already after a *single asymmetric fission event*. Even larger enhancement in the surface-active compounds can be expected if the progeny droplet itself goes through another fission event. For less surface-active compounds, which distribute more uniformly between the droplet surface and interior, the enhancement will be smaller.

Why are these observations significant? Aerosolization of solutions with EAG devices finds increasing use in various applications including aerosol-assisted nanomaterial synthesis (Lu et al. 1999; Jaworek and Sobczyk 2008), targeted drug delivery (Tang and Gomez 1994; Chattopadhyay et al. 2010), and mobility analysis of colloids (Lenggoro et al. 2002; Ude et al. 2006), proteins, (Szymanski et al. 2001) and viruses (Tito et al. 2000; Thomas et al. 2004; Eninger et al. 2009; Pease et al. 2009). We have shown that the chemical composition of the nanoparticles produced by an EAG may be quite sensitive to the operation conditions and not necessarily reflect the distribution of solutes in the initial solution. If the spray is not neutralized promptly, the surface-active species may become significantly enriched in the nanoparticles. As the enrichment occurs during fission of the highly charged particles, it is difficult to fully suppress this effect because at least some fission is necessary to break down the droplets produced from the electrospray cone. Therefore, we anticipate that surface-active species will always be enriched to some extent in EAG-generated nanoparticles, regardless of the specifics of the EAG design. The EAG users should be mindful of this effect and design their experiments appropriately to compensate for it.

REFERENCES

Alshawa, A., Dopfer, O., Harmon, C. W., Nizkorodov, S. A., and Underwood, J. S. (2009). Hygroscopic Growth and Deliquescence of NaCl Nanoparticles Coated with Surfactant AOT. *J. Phys. Chem. A*, 113:7678–7686.

Benkestock, K., Sundqvist, G., Edlund, P.-O., and Roeraade, J. (2004). Influence of Droplet Size, Capillary-Cone Distance and Selected Instrumental Parameters for the Analysis of Noncovalent Protein-Ligand Complexes by Nano-Electrospray Ionization Mass Spectrometry. *J. Mass Spectrom.*, 39:1059–1067.

Biskos, G., Malinowski, A., Russell, L., Buseck, P., and Martin, S. (2006a). Nanosize Effect on the Deliquescence and the Efflorescence of Sodium Chloride Particles. *Aerosol Sci. Technol.*, 40:97–106.

Biskos, G., Russell, L. M., Buseck, P. R., and Martin, S. T. (2006b). Nanosize Effect on the Hygroscopic Growth Factor of Aerosol Particles. *Geophys. Res. Lett.* 33:L07801, doi:07810.01029/005GL025199.

Cech, N. B., and Enke, C. G. (2001). Practical Implications of Some Recent Studies in Electrospray Ionization Fundamentals. *Mass Spectrom. Rev.*, 20:362–387.

Chattopadhyay, S., Modesto-Lopez, L. B., Venkataraman, C., and Biswas, P. (2010). Size Distribution and Norphology of Liposome Aerosols Generated by Two Methodologies. *Aerosol Sci. Technol.*, 44:972–982.

Chen, D.-R., Pui, D. Y. H., and Kaufman, S. L. (1995). Electrospraying of Conducting Liquids for Monodisperse Aerosol Generation in the 4 nm to 1.8 mm Diameter Range. *J. Aerosol Sci.*, 26:963–977.

Eninger, R. M., Hogan, C. J., Jr., Biswas, P., Adhikari, A., Reponen, T., and Grinshpun, S. A. (2009). Electrospray Versus Nebulization for aerosolization and filter testing with bacteriophage particles. *Aerosol Sci. Technol.*, 43:298–304.

Hameri, K., Laaksonen, A., Vakeva, M., and Suni, T. (2001). Hygroscopic growth of ultrafine sodium chloride particles. *J. Geophys. Res. D*, 106:20749–20757.

Harmon, C. W., Grimm, R. L., McIntire, T. M., Peterson, M. D., Njegic, B., Angel, V. M. et al. (2010). Hygroscopic growth and deliquescence of NaCl nanoparticles mixed with surfactant SDS. *J. Phys. Chem. B*, 114:2435–2449.

Iyota, H., and Krastev, R. (2009). Miscibility of sodium chloride and sodium dodecyl sulfate in the adsorbed film and aggregate. *Colloid Polym. Sci.*, 287:425–433.

Jaworek, A., and Sobczyk, A. T. (2008). Electrospraying route to nanotechnology: An overview. *J. Electrostatics*, 66:197–219.

Kebarle, P., and Peschke, M. (2000). On the mechanisms by which the charged Droplets produced by electrospray lead to gas phase ions. *Analyt. Chim. Acta*, 406:11–35.

Kebarle, P., and Verkerk, U. H. (2010). On the Mechanism of Electrospray Ionization Mass Spectrometry (ESIMS), in *Electrospray and MALDI Mass Spectrometry: Fundamentals, Instrumentation, Practicalities, and Biological Applications*, R. B. Cole, ed., John Wiley & Sons, Inc., Hoboken, NJ, p. 863.

Lenggoro, I. W., Xia, B., Okuyama, K., and Fernandez de la Mora, J. (2002). Sizing of Colloidal Nanoparticles by Electrospray and Differential Mobility Analyzer Methods. *Langmuir*, 18:4584–4591.

Lu, Y., Fan, H., Stump, A., Ward, T. L., Rieker, T., and Brinker, C. J. (1999). Aerosol-Assisted Self-Assembly of Mesostructured Spherical Nanoparticles. *Nature*, 398:223–226.

Lu, Q., and Koropchak, J. A. (2004). Corona Discharge Neutralizer for Electrospray Aerosols used with Condensation Nucleation Light-Scattering Detection. *Analyt. Chem.*, 76:5539–5546.

Modesto-Lopez, L. B., Kettleson, E. M., and Biswas, P. (2011). Soft X-Ray Charger (SXC) System for use with Electrospray for Mobility Measurement of Nioaerosols. *J. Electrostatics*, 69:357–364.

Pease, L. F., III, Lipin, D. I., Tsai, D.-H., Zachariah, M. R., Lua, L. H. L., Tarlov, M. J. et al. (2009). Quantitative Characterization of Virus-Like Particles by Asymmetrical Flow Field Flow Fractionation, Electrospray Differential Mobility Analysis, and Transmission Electron Microscopy. *Biotech. Bioengineering*, 102:845–855.

Rader, D. J., and McMurry, P. H. (1986). Application of the Tandem Differential Mobility Analyzer to Studies of Droplet Growth or Evaporation. *J. Aerosol Sci.*, 17:771–787.

Rulison, A., and Flagan, R. C. (1994). Electrospray Atomization of Electrolytic Solutions. *J. Colloid Interface Sci.*, 167:135–145.

Scalf, M., Westphall, M. S., Krause, J., Kaufman, S. L., and Smith, L. M. (1999). Controlling Charge States of Large Ions. *Science*, 283:194–197.

Schmidt, A., Karas, M., and Dülcks, T. (2003). Effect of Different Solution Flow Rates on Analyte Ion Signals in Nano-ESI MS, or: When does ESI Turn into Nano-ESI? *J. Am. Soc. Mass. Spectrom.*, 14:492–500.

Sperline, R. P. (1997). Infrared Spectroscopic Study of the Crystalline Phases of Sodium Dodecyl Sulfate. *Langmuir*, 13:3715–3726.

Stokes, R. H., and Robinson, R. A. (1966). Interactions in Aqueous non-electrolyte solutions. I. Solute-solvent equilibriums. *J. Phys. Chem.*, 70:2126–2131.

Stolzenburg, M. R., and McMurry, P. H. (1988). *TDMAFIT Unser's Manual (PTL Publication No. 653)*. Particle Technology Laboratory, Univeristy of Minnesota, Minneapolis, MN, USA, p. 61.

Svenningsson, B., Rissler, J., Swietlicki, E., Mircea, M., Bilde, M., Facchini, M. C. et al. (2006). Hygroscopic Growth and Critical Supersaturations for Mixed Aerosol Particles of Inorganic and Organic Compounds of Atmospheric Relevance. *Atm. Chem. Phys.*, 6:1937–1952.

Szymanski, W. W., Bacher, G., and Allmaier, G. (2001). Nano-Aerosol Approach for Characterization of Proteins and Viruses. *Proc. SPIE-The Int. Soc.Optical Eng.*, 4590:38–44.

Tang, K., and Gomez, A. (1994). Generation by Electrospray of Monodisperse Water Droplets for Targeted Drug Delivery by Inhalation. *J. Aerosol Sci.*, 25:1237–1249.

Tang, K., and Smith, R. D. (2001). Physical/Chemical Separations in the Break-up of Highly Charged Droplets from Electrosprays. *J. Am. Soc. Mass. Spectrom.*, 12:343–347.

Taylor, G. (1964). Disintegration of Water Drops in an Electric Field. *Proc. Royal Soc. London. A. Math. Phys. Sci.*, 280:383–397.

Thomas, J. J., Bothner, B., Traina, J., Benner, W. H., and Siuzdak, G. (2004). Electrospray ion Mobility Spectrometry of Intact Viruses. *Spectroscopy*, 18:31–36.

Tito, M. A., Tars, K., Valegard, K., Hajdu, J., and Robinson, C. V. (2000). Electrospray Time-of-Flight Mass Spectrometry of the Intact MS2 Virus Capsid. *J. Am. Chem. Soc.*, 122:3550–3551.

Ude, S., Fernandez de la Mora, J., Alexander, J. N., and Saucy, D. A. (2006). Aerosol Size Standards in the Nanometer Size Range. II. Narrow Size Distributions of Polystyrene 3–11 nm in Diameter. *J. Colloid Interface Sci.*, 293:384–393.

Varutbangkul, V., Brechtel, F. J., Bahreini, R., Ng, N. L., Keywood, M. D., Kroll, J. H. et al. (2006). Hygroscopicity of Secondary Organic Aerosols Formed by Oxidation of Cycloalkenes, Monoterpenes, Sesquiterpenes, and Related Compounds. *Atm. Chem. Phys.*, 6:2367–2388.

Zelenyuk, A., Imre, D., Cuadra-Rodriguez, L. A., and Ellison, B. (2007). Measurements and Interpretation of the Effect of a Soluble Organic Surfactant on the Density, Shape and Water Uptake of Hygroscopic Particles. *J. Aerosol Sci.*, 38:903–923.